Mon. Not. R. astr. Soc. (1992) **255**, 431–440

The spectral signature of the cooling flow in Abell 478

R. M. Johnstone,[1] A. C. Fabian,[1] A. C. Edge[1] and P. A. Thomas[2]
[1] *Institute of Astronomy, Madingley Road, Cambridge CB3 0HA*
[2] *Astronomy Centre, University of Sussex, Falmer, Brighton BN1 9QH*

Accepted 1991 October 29. Received 1991 October 28; in original form 1990 September 7

SUMMARY

We present X-ray spectra of Abell 478 taken with the *Ginga* LAC and with the *Einstein* SSS. The LAC data set an upper limit of $\sim 440\ M_\odot\ \mathrm{yr}^{-1}$ on the mass deposition rate throughout the whole cluster if a value for the galactic absorption based on 21-cm observations of H I is adopted. The SSS data strongly require an absorbing column density well in excess of that expected by scaling from 21-cm observations of galactic H I. Data from the LAC, SSS and HRI taken together imply a mass deposition rate of about $1000\ M_\odot\ \mathrm{yr}^{-1}$ with an absorption column density $\sim 4.8 \times 10^{21}\ \mathrm{cm}^{-2}$. The excess absorption may be intrinsic to the cooling flow or due to structure in the interstellar medium of the Galaxy on a scale smaller than the grid of 21-cm observations.

1 INTRODUCTION

X-ray images of most clusters of galaxies show the emission to be peaked around the central galaxy. For any reasonable gravitational potential well, this means that the gas there is much denser and cooler than in the general intracluster medium. The radiative cooling time of the central gas is usually shorter than the expected age of the cluster, $t_a \sim 10^{10}$ yr. The cooling gas must then flow inward in order to maintain the pressure necessary to support the weight of the overlying gas; a cooling flow is formed (for reviews see Fabian, Nulsen & Canizares 1984; Sarazin 1986; Fabian, Nulsen & Canizares 1991). In most cases the mass deposition rate of cooled gas, $\dot{M}$, is at least $10\ M_\odot\ \mathrm{yr}^{-1}$, for many it exceeds $100\ M_\odot\ \mathrm{yr}^{-1}$, and, for a few, $\dot{M} \gtrsim 500\ M_\odot\ \mathrm{yr}^{-1}$ (Stewart *et al.* 1984; Thomas, Fabian & Nulsen 1987; Arnaud 1988; Pesce *et al.* 1990; Edge, Stewart & Fabian 1992).

The cooling rate is generally estimated from the observed X-ray luminosity within the cooling radius, r_{cool}, where the cooling time of the gas equals the assumed age of the cluster, t_a. Essentially, $\dot{M}$ is of order the mass of gas within r_{cool} divided by t_a. Independent evidence for the presence of cooling flows is provided by high-resolution X-ray spectra of a few bright clusters. These show emission-lines characteristic of gas at temperatures below 10^7 K in quantities consistent with that expected from the imaging estimates (Canizares, Markert & Donahue 1988, and references therein).

The surface brightness profiles of the clusters indicate that $\dot{M}$ varies with radius, r, in a systematic manner such that $\dot{M}(<r) \propto r$, approximately. If the cooling gas is present as a single phase (i.e. at each radius it has a unique temperature and density) the surface brightness would be even higher and more centrally condensed than is observed. The observed surface brightness profiles therefore imply that the cooling gas exists as a multiphase medium in which there is a broad range of densities (and temperatures) present at all radii (Nulsen 1986). The spectrum of the densities present at large radii and its radial dependence are the key diagnostics of the flow parameters. The measurement of these quantities would not only determine the total mass deposition rate, $\dot{M}_{\mathrm{total}}$, but also provide some guide to how the gas behaves when subclusters merge; it would probe the past history of a cluster. The temperature of the intracluster gas near r_{cool} is generally considered to be close to the mean temperature of the outer cluster gas. Thomas *et al.* (1987) have shown that the density contrast $\delta\rho/\rho[\propto(\delta T/T)^{-1}]$ needs to be at least a factor of 2 at large radii in order to give the observed mass deposition profiles.

The signature of this cooling gas should be evident in the 2–10 keV spectrum of a massive cooling flow as an additional spectral component, cooler than the ambient cluster gas. Mushotzky & Szymkowiak (1988) have found evidence for cool spectral components in the cores of eight clusters using lower energy (0.6–4.5 keV) spectra of clusters taken with the *Einstein Observatory* Solid State Spectrometer (SSS). Their mass deposition rates inferred from fitting a range of cooling models are in good agreement with those determined independently from the imaging data. Unrestrictive upper limits are given for two other clusters for which they did not have imaging data to compare with. Further evidence for cool components ($T \sim 3 \times 10^6$ K) in the Virgo and Perseus clusters was found by Canizares *et al.* (1988) using the *Ein-*

stein Observatory Focal Plane Crystal Spectrometer. The cooling time for these components ($\sim 10^8$–10^9 yr) is much shorter than the Hubble time.

Little evidence has been found for the signature of cooling gas in previous work which fitted multicomponent spectral models to 2–10 keV spectra of clusters. There is evidence for hard and soft components in the Centaurus and Hydra (Abell 1060) clusters (Mitchell & Mushotzky 1980), but, although these two clusters do contain cooling flows, their mass deposition rates are low (22 and 6 $M_\odot$ yr^{-1}; Fabian, Nulsen & Canizares 1984; Stewart *et al.* 1984, respectively). The soft (low-temperature) components found correspond to those expected from the ambient gas in such low-richness clusters (Edge & Stewart 1991), indicating that the hard component may be due to an active nucleus like that seen in the X-ray spectrum of the Cygnus-A cluster (Arnaud *et al.* 1987). Hughes *et al.* (1988) have reported that the temperature decreases outward in the Coma cluster. The imaging data for this cluster do not show an obvious cooling flow, although there could be a disrupted or distributed cooling flow of up to 125 $M_\odot$ yr^{-1} (Fabian, Nulsen & Canizares 1984; Canizares, Markert & Donahue 1988).

In this paper, we measure the mass deposition rate in Abell 478 using X-ray spectra taken with the *Ginga* Large Area proportional Counters (LAC), and the *Einstein Observatory* Solid State Spectrometer (SSS), and compare these values with those obtained by deprojecting the *Einstein Observatory* High Resolution Imager (HRI) data. We have selected Abell 478 since it has a massive flow with $\dot{M} \sim 500$ $M_\odot$ yr^{-1} (Arnaud 1986; Thomas *et al.* 1987; Edge & Stewart 1991) and is a cluster which does not also contain a powerful radio source (Valentijn & Bijleveld 1983). [Radio sources in central cluster galaxies may indicate the presence of an active nucleus which would have a corresponding power-law component in the X-ray band, as observed in the Perseus, Virgo (M87) and Cygnus-A clusters.] In Section 2 we review the spectrum of the cooling gas. In Section 3 we present the new *Ginga* X-ray spectrum of Abell 478 and in Section 4 we analyse the SSS spectra from the *EXOSAT* database. Finally, in Section 5 we discuss the implications of the spectral fits to the Abell 478 data. There is strong evidence for extra absorption in the X-ray spectra of Abell 478 over and above the measured galactic column. This complicates the spectral measurement of the cooling flow, but we nevertheless find a result in good agreement with the X-ray imaging data, showing that Abell 478 is one of the strongest cooling flows known.

2 THE SPECTRUM OF COOLING GAS

In a cooling flow, gas cools continually from some upper temperature $T_{\max}$, so that at any instant the spectrum of the cooling gas is given by the sum of the luminosities of the gas present at all temperatures below $T_{\max}$. The amount of gas at each temperature is controlled by how rapidly the gas can cool at each temperature. The equations giving the emissivity of the cooling gas in a single spectral line were presented by Canizares *et al.* (1988). Here we review the equations adapted to a form relevant to the integrated spectrum of a cluster.

A volume V of gas at density n cooling at constant pressure from temperature T to $T-dT$ emits a luminosity

$$dL_{\rm cool} = n_{\rm e} n_{\rm H} \Lambda(T)\, dV = \frac{5}{2}\frac{\dot{M}}{\mu m_{\rm H}}\, k\, dT, \qquad (1)$$

where $\dot{M}$ is the mass deposition rate, $n_{\rm e}$ and $n_{\rm H}$ are the electron and proton densities, μ is the mean molecular weight of the gas, $m_{\rm H}$ is the mass of the hydrogen atom, k is the Boltzmann constant and $\Lambda(T)$ is the value of the cooling function at temperature T.

The luminosity of the spectrum at each frequency is

$$dL_{\rm cool}(\nu) = n_{\rm e} n_{\rm H} \varepsilon_\nu dV \qquad (2)$$

where ε_ν is the emissivity at frequency ν.

Substituting for $n_{\rm e} n_{\rm H} dV$ and integrating we obtain

$$L_{\rm cool}(\nu) = \frac{5k}{2\mu m_{\rm H}}\dot{M}\int_0^{T_{\max}} \frac{\varepsilon_\nu}{\Lambda(T)}\, dT. \qquad (3)$$

The cooling spectrum is therefore simply the summation of the emissivity at each temperature weighted inversely by the value of the cooling function at that temperature. The normalization is set by the mass deposition rate. There are two free parameters which control the shape of the spectrum, namely $T_{\max}$, the temperature that the gas cools from, and the metal abundance which changes the emissivity and cooling function at each temperature. A practical lower limit of 10^6 K is used for our grid of cooling models in the $T_{\max}$/metal abundance plane.

The mass deposition rate in equation (1) corresponds directly to the mass deposition rate inferred from the deprojection analysis of X-ray images of clusters, e.g. Fabian *et al.* (1981) if data within the same radii are considered in both analyses. In the case of the image deprojection, the mass deposition rate is calculated only within that part of the image within $r_{\rm cool}$ where the cooling time is less than the age of the cluster.

In an idealized homogeneous cooling flow, the gas has only one temperature and one density at each radius and the cooling radius is well defined. In practice, the surface brightness profiles indicate that the intracluster medium is multiphase, with gas having a range of densities and temperatures and existing in pressure equilibrium at each radius, at least within the cooling radius. In this case, the mass deposition rate can be calculated out to where the cooling time of the gas, averaged over the individual phases, is equal to the age of the cluster. Thomas *et al.* (1987) have shown that it is possible to determine the distribution of densities from the *Einstein* images with highest signal-to-noise ratios. This density distribution is in fact the same as that which gives rise to the spectrum in equation (3). Furthermore, they find that, taking into account the multiphase gas, the deprojection analysis gives mass deposition rate profiles very similar to those from the simple homogeneous single-phase approach, out to the cooling radius. There may, however, be further gas cooling beyond the phase-averaged cooling radius, but the total amount cannot be inferred from the imaging data without a detailed model for the distribution of gas density as a function of radius throughout the cluster.

The integrated spectrum of the cluster is potentially sensitive to all the gas which is cooling within the cluster without regard to its spatial distribution, and can give the maximum mass deposition rate for the cluster. Such an estimate of the mass deposition rate is strictly an upper limit as the spectrum

(as measured with a proportional counter) is not sensitive to the density of gas which is giving rise to it. A spectrum identical to that from cooling gas is indeed expected from the density distribution inferred to exist at r_{cool} by Thomas *et al.* (1987).

3 THE *GINGA* SPECTRUM OF ABELL 478

3.1 *Ginga* observations and data reduction

The *Ginga* data on Abell 478 were taken on 1989 February 7. Background subtraction techniques outlined in Hayashida *et al.* (1989) were used with the inclusion of additional radioactive decay features in the instrument. The time-dependent background model was developed using blank sky observations taken over a period of four weeks centred on the Abell 478 observation. After the exclusion of periods of high background a total exposure time of 24 900 s on source was obtained at a count rate of ~30.4 count s^{-1} (~2–20 keV) in the top counter layer. Uncertainties in the data were calculated from the counting statistics but with the inclusion of an extra 0.5 per cent added in quadrature to account for systematic errors in the response matrix. The count rate in the mid-layer never exceeds that in the top layer at any energy, so that systematic errors due to the background subtraction are always larger in the mid-layer. In the following analysis we have therefore fitted only the spectrum from the top layer of the *Ginga* LAC.

3.2 Isothermal model

We first fitted the *Ginga* data with an isothermal, optically thin, plasma-emission model based on the work of Raymond & Smith (1977), with line-of-sight photoelectric absorption using cross-sections from Morrison & McCammon (1983). The redshift is not well constrained by the *Ginga* data which formally allow $z=0.082^{+0.023}_{-0.005}$. (We quote the 90 per cent confidence region for a single interesting parameter, unless otherwise stated.) We have therefore fixed the redshift at the optically measured value of $z=0.088$ (Zabludoff, Huchra & Geller 1990).

The best-fitting Raymond–Smith model gives a temperature corresponding to $kT=6.84^{+0.20}_{-0.24}$ keV, a metal abundance of 0.37 ± 0.04 of the cosmic value and a galactic absorption column density corresponding to $N_H=1.6^{+1.3}_{-1.1}\times10^{21}$ cm^{-2}. This model gives a value of the chi-square statistic of 28.1 for the 31 PHA channels and a 2–10 keV flux of $6.30\pm0.04\times10^{-11}$ erg cm^{-2} s^{-1}. In the rest frame of the cluster the 2–10 keV luminosity is 2.3×10^{45} erg s^{-1} (after removing the line-of-sight absorption and using $H_0=50$ km s^{-1} Mpc^{-1} and $q_0=0.0$). In Fig. 1(a) we show the observed spectrum (crosses) together with the best-fitting model folded through the detector response (solid line). Fig. 1(b) shows the residuals from the best-fitting model.

The *Ginga* spectrum does not tightly constrain the galactic column density. A simple analysis of the 21-cm observations (Stark *et al.*, private communication) gives a column density of 1.2×10^{21} cm^{-2}, but Heiles (private communication) indicates that the line is slightly optically thick and that a better estimate of the column density is $N_H\approx2.0\times10^{21}$ cm^{-2}. We note, however, that the bright star HD26676 which lies within 20 arcmin of the centre of the cluster has a bright reflection nebulosity of radius ~35 arcmin around it (Centurion & Vladido 1989). There may therefore be additional interstellar material on small angular scales not measured by the 21-cm observations.

3.3 Power-law component

We have checked for the presence of an X-ray power-law component arising from an active nucleus by trying to fit the spectrum with an additional absorbed power-law component. The known power-law components in the Perseus, Virgo (M87) and Cygnus-A clusters are heavily absorbed at low energies. Constraining the power law to have a photon number index of 1.7, typical of many active galactic nuclei (Turner & Pounds 1989), we find that the best-fitting model requires no power-law component, with a 90 per cent (single-parameter) upper limit on the 2–10 keV flux of 1.97×10^{-12} erg cm^{-2} s^{-1}. The upper limit to the 2–10 keV (rest-frame) luminosity, including the absorption of $N_H\sim2\times10^{23}$ cm^{-2} on the power law is 6.3×10^{43} erg s^{-1}, which corresponds to an intrinsic luminosity of 1.5×10^{44} erg s^{-1}. These luminosities correspond to 3 and 6 per cent of the cluster luminosity, respectively.

3.4 Cooling flow component

In order to determine the contribution to the total cluster emission from the cooling flow we have fitted the data with a single-temperature Raymond–Smith model, to account for the ambient cluster gas, plus model cooling spectra. The normalizations of the two spectral components are free-fit parameters which correspond to the emission measure and mass deposition rate for the two components respectively. The two model components were constrained to have the same element abundances, and the upper temperature from which the gas cools, T_{max}, was assumed equal to $T_{cluster}$, the ambient cluster temperature. The normalization of the two components are free-fit parameters related to the fluxes received from the ambient and the cooling cluster gas.

Fixing the galactic absorbing column at 2×10^{21} cm^{-2} gives a value of $\chi^2=28.3$ and yields a mass deposition rate of 66^{+376}_{-66} $M_\odot$ yr^{-1}, i.e. less than 442 $M_\odot$ yr^{-1}. The allowed range on the mass deposition rate deduced from the LAC data depends strongly on the galactic absorption. Fig. 2 shows contours of the increase in chi-square (solid line) as the mass deposition rate and the galactic absorption column density are changed from their best-fitting values ($\dot{M}=0$ $M_\odot$ yr^{-1}, $N_H=1.6\times10^{21}$ cm^{-2}; indicated by the filled circle). They correspond to $\Delta\chi^2=4.61$ and 9.21 which shows the 90 and 99 per cent confidence regions for the two parameters.

The mass deposition rate calculated from the X-ray imaging data from the *Einstein Observatory* HRI (Thomas *et al.* 1987) and *EXOSAT* LE (Edge & Stewart 1991) is ~500 $M_\odot$ yr^{-1}, where the H I column was fixed at $N_H=1.2\times10^{21}$ cm^{-2}, and $t_a=2.0\times10^{10}$ yr. The *Ginga* data are only marginally consistent with these results. In the light of our new data, we have re-analysed the *Einstein Observatory* High Resolution Imager (HRI) data using several values of N_H, the best optical redshift for the cluster (Zabludoff *et al.* 1990) and assuming that $t_a=10^{10}$ yr. [We used the single-phase method of Fabian *et al.* (1981) which Thomas *et al.* (1987) have shown gives very similar mass deposition rates to the multiphase method.] The filled circles with error bars in Fig.

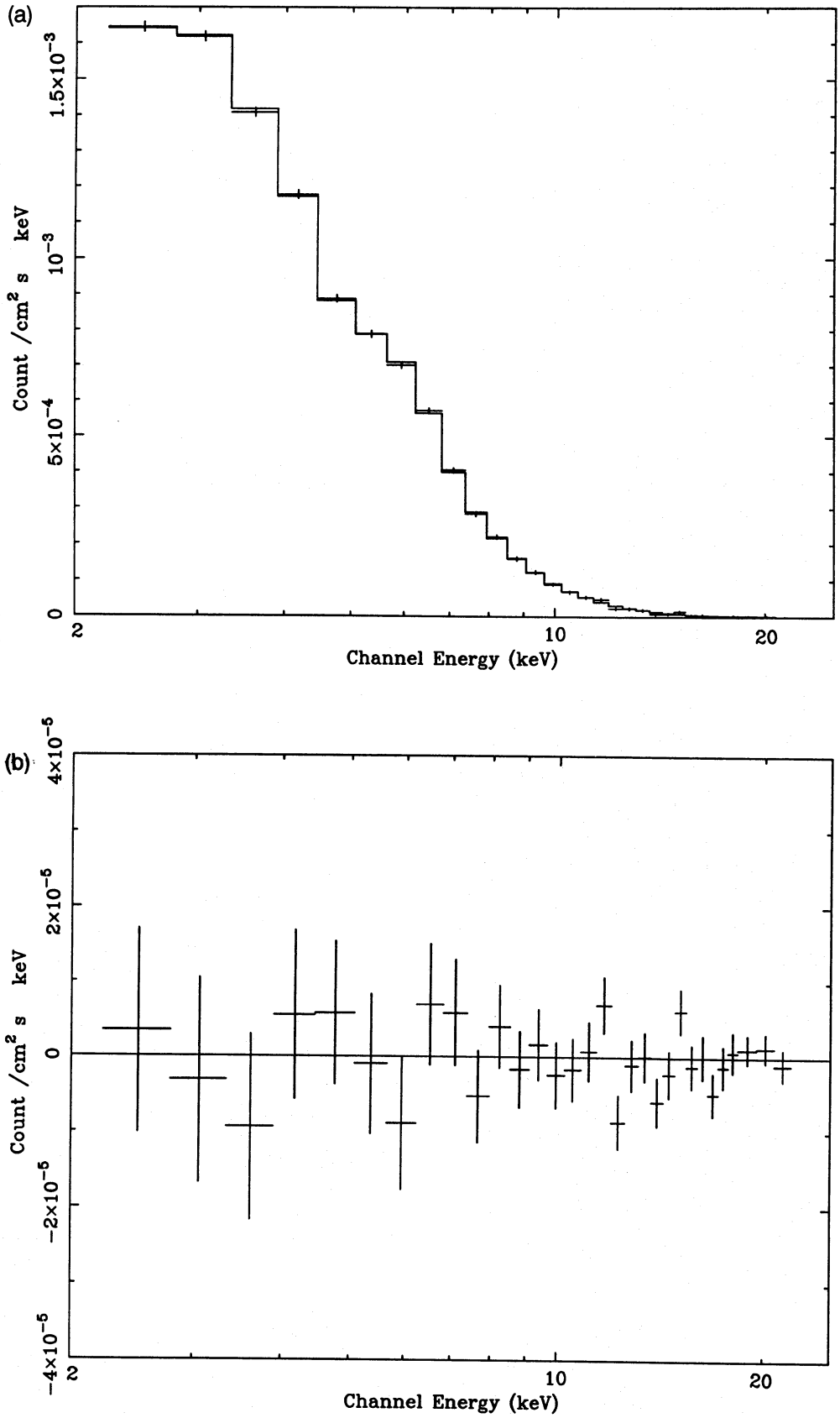

Figure 1. (a) The *Ginga* spectrum of Abell 478 (crosses) with the best-fitting isothermal plasma-emission model folded through the detector response overlaid (solid line). (b) Residuals of the data from the best-fitting model.

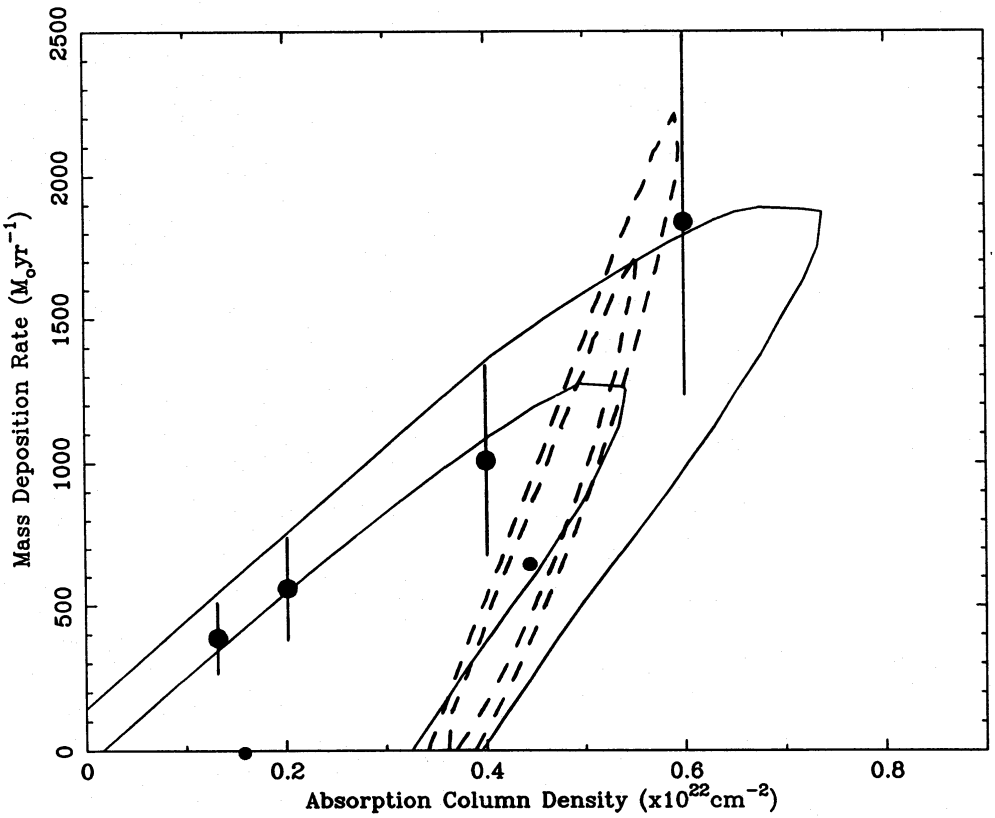

Figure 2. Contours of increasing chi-square in the mass-deposition rate/absorption column density plane, deduced from the *Ginga* spectrum (solid contours) and SSS data (dashed contours). The two contours are at $\chi^2_{min}+4.61$ and $\chi^2_{min}+9.21$ which correspond to the 90 and 99 per cent confidence regions for two interesting parameters. The filled circles show the best-fitting value of the parameters. The filled circles with error bars show the mass deposition rates deduced from the HRI data with different assumed absorption. These errors indicate the likely size of systematic uncertainties.

2 indicate the mass deposition rates calculated from the HRI data as a function of absorption column density. The error bars show the possible systematic uncertainties in the image analysis, such as the assumed gravitational potential well, which can introduce an error of ±30 per cent (Arnaud 1988).

4 THE *EINSTEIN* SSS SPECTRA OF ABELL 478

4.1 SSS observations

The SSS data on Abell 478 were extracted from the *EXOSAT* database. An important feature of the analysis of SSS data is the correction for the build-up of ice on the detector window. The response matrix available from the *EXOSAT* database incorporates a correction for the ice, calculated from a detailed model based on fitting the spectrum of the Crab nebula. Details of the model used are given by Arnaud, Szymkowiak & White (1989) and are summarized in Turner *et al.* (1991). The amount of ice on the detector window is calculated from this model and given by the ice parameter.

There are five SSS observations of Abell 478 in the *EXOSAT* database. We have chosen to analyse only the three observations taken on day numbers 1979 246, 268 and 249. The previous two observations, taken on day numbers 1979 49 and 50 have much more ice on the detector window and were taken outside the period over which the ice model is known to be valid. Turner *et al.* (1991) have shown, from a comparison of SSS and Monitor Proportional Counter data of (point-source) active galactic nuclei, that the error in the ice parameter is less than ±20 per cent. This corresponds to an error in the effective area of the SSS of ±20 per cent at 600 eV or ±14 per cent at 1 keV.

Table 1 gives other details of the observations including the exposure time and the value of the ice parameter. The uncertainties associated with the PHA data available from the *EXOSAT* database include an extra 2 per cent added to the counting statistics in quadrature to account for systematic errors in the response matrix and ice correction.

The SSS background contains two components (Szymkowiak 1985; Turner *et al.* 1991). The dominant component, due to the particle background, can be subtracted directly by scaling blank-sky observations using spacecraft telemetry. The second component is thought to be due to electronics. This component has a constant spectral shape, but an unpre-

Table 1. SSS observations of Abell 478.

Date	Exposure (S)	Ice parameter
1979/246	9256	0.44
1979/248	2621	0.82
1979/249	3194	0.83

dictable intensity and is accounted for by subtracting a correction spectrum. The fitting procedure is then as follows: a spectral model is fitted to the data and the normalizations of the correction files are adjusted to reduce chi-squared. This procedure is repeated allowing the model parameters to vary until the value of the chi-square statistic is minimized.

4.2 Isothermal model

The SSS (Giacconi *et al.* 1979; Holt *et al.* 1979) is sensitive in the energy range 0.5–4.5 keV, and is unable to measure the cluster temperature accurately. We have therefore set the temperature of the isothermal model at that measured by *Ginga*. We also set the metal abundance to that measured by *Ginga* and the redshift to the optically measured value of $z=0.088$. In contrast to the *Ginga* spectrum, the SSS data are very sensitive to the absorption column. Fixing this at the value estimated from the 21-cm observations of H I (2.0×10^{21} cm^{-2}) gives a very poor fit: $\chi^2=575.0$ for 237 PHA channels. Fig. 3 shows the SSS data (where data from the three observations have been binned together for presentation) with this model (solid line) overlaid. When the absorption is allowed to vary, we find that the model requires a value of $N_{\rm H}=3.6\pm0.2\times10^{21}$ cm^{-2}, reducing the chi-square statistic to $\chi^2=228.8$ for 237 PHA channels. This model gives an observed 0.5–4.5 keV flux of $3.54\pm0.08\times10^{-11}$ erg cm^{-2} s^{-1}, and a 0.5–4.5 keV luminosity of 1.8×10^{45} erg s^{-1} in the rest frame of the cluster. Extrapolation of the spectrum gives a predicted 2–10 keV flux of $4.05\pm0.11\times10^{-11}$ erg cm^{-2} s^{-1}, and a 2–10 keV luminosity of 1.7×10^{45} erg s^{-1} in the rest frame of the cluster.

4.3 Cooling flow model

Addition of a cooling flow component to the isothermal model produces a further decrease in chi-square. We have allowed the normalization of the isothermal component and the mass deposition rate of the cooling flow component to be free fitting parameters. The temperature and abundances were forced to match those of the ambient cluster gas temperature as measured by *Ginga*. This gives a reduction in chi-square of 3.9 for only one further fitting parameter, which is significant at more than the 95 per cent level. The best-fitting value of the mass deposition rate is $\dot{M}=680^{+790}_{-580}\ M_\odot$ yr^{-1}. This model requires an increase in the absorption column density to $N_{\rm H}=4.5\pm0.8\times10^{21}$ cm^{-2}. The SSS data with this model overlaid are shown in Fig. 4(a). In Fig. 4(b) we plot the residuals from this model. Further, allowing the abundance of the cooling flow component to be a free parameter only reduces chi-square by a further 1.8. This formally gives an abundance of $0.66^{+0.39}_{-0.31}$ but the reduction in chi-square is too small for the data to require the abundance to be a free parameter. The inclusion of the correction spectrum reduced the value of chi-square by 13.0. The 0.5–4.5 keV fluxes of the isothermal and cooling flow components are respectively $(2.5\pm0.9)\times10^{-11}$ and $(1.0\pm0.8)\times10^{-11}$ erg cm^{-2} s^{-1} corresponding to 0.5–4.5 keV luminosities emitted in the

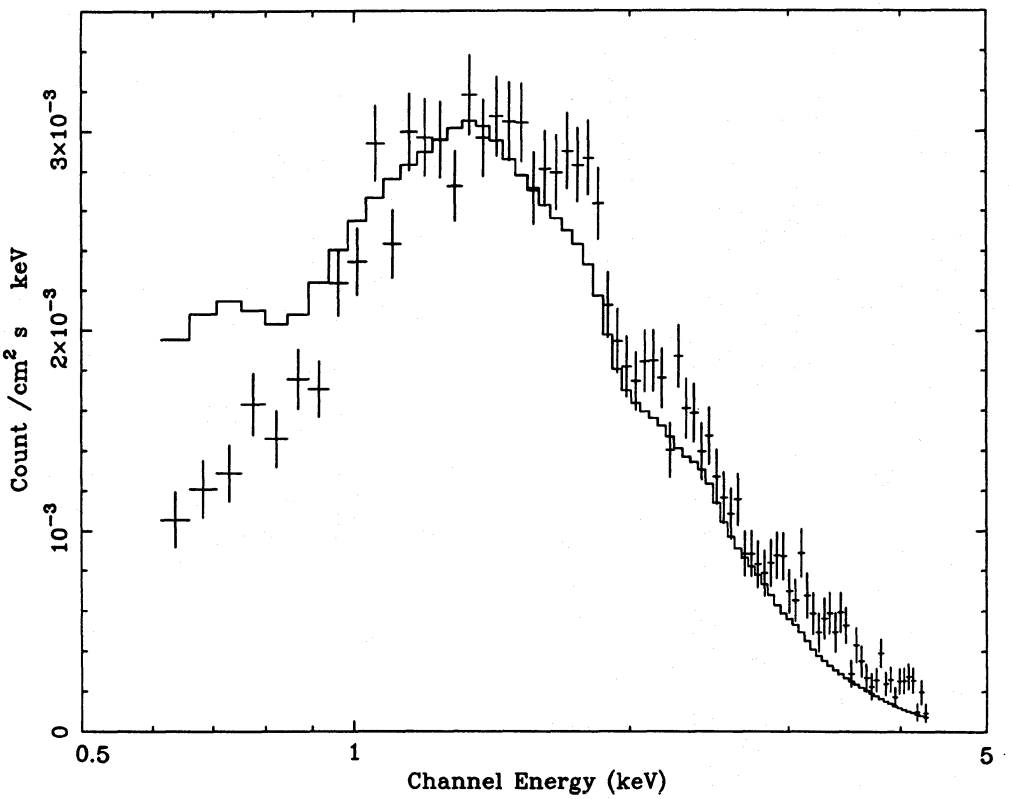

Figure 3. The SSS spectrum of Abell 478 (crosses). The solid lines shows an isothermal model with the temperature and abundance measured by the LAC, with photoelectric absorption corresponding to the galactic value of $N_{\rm H}=2.0\times10^{21}$ cm^{-2}, renormalized to fit the SSS data, folded through the detector response.

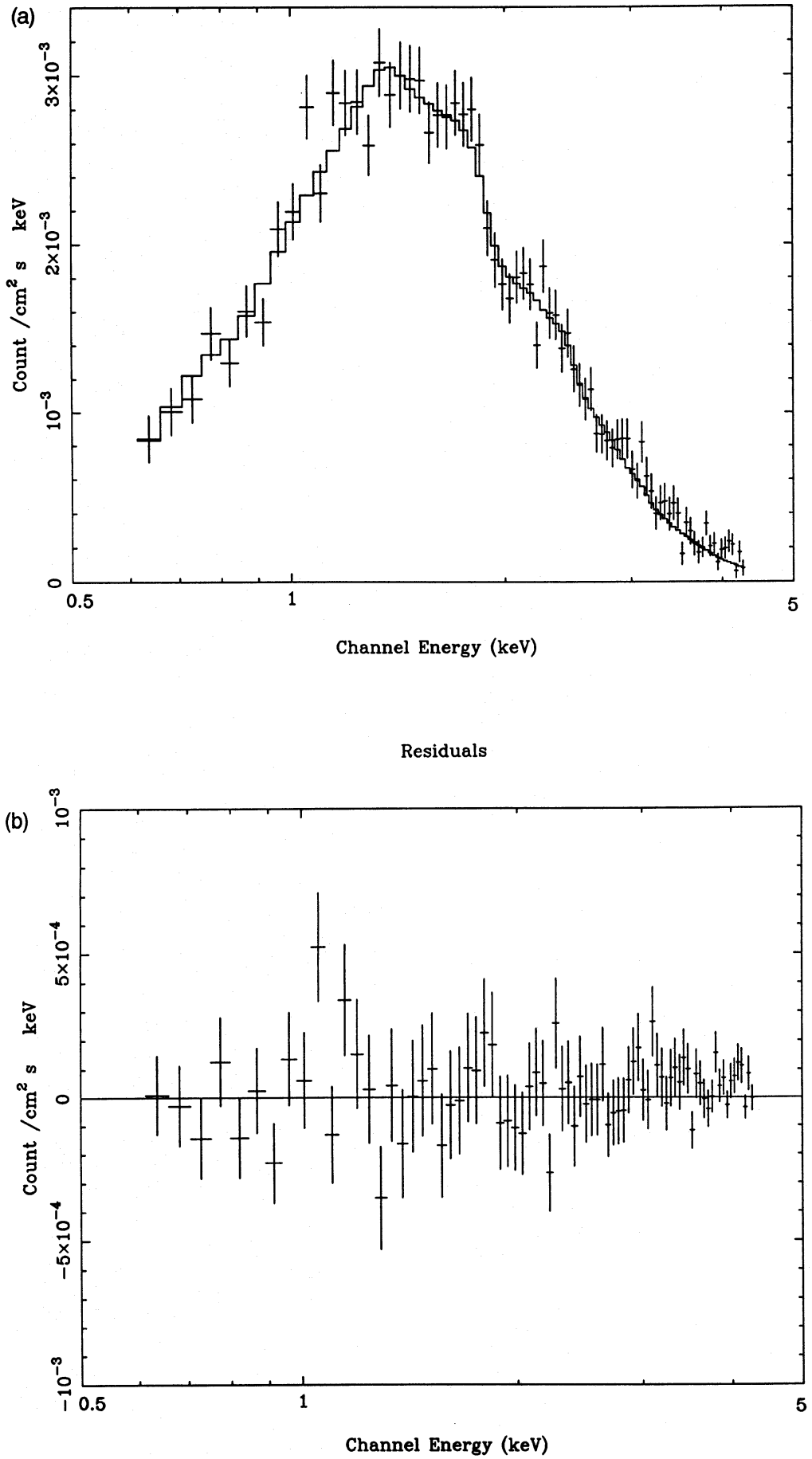

Figure 4. (a) The SSS spectrum of Abell 478 (crosses) with the best-fitting isothermal plus cooling flow model and freely fitted photoelectric absorption, folded through the detector response, overlaid (solid line). (b) Residuals of the data from the best-fitting model.

rest frame of 1.3×10^{45} and 6.6×10^{44} erg s^{-1}. Extrapolation of the spectra gives predicted 2–10 keV fluxes of $(3.2\pm1.1)\times10^{-11}$ and $(9\pm8)\times10^{-12}$ erg cm^{-2} s^{-1} with corresponding 2–10 keV luminosities in the rest frame of 1.3×10^{45} and 3.7×10^{44} erg s^{-1}.

In order to determine how sensitive our result is to the precise value used for the ice parameter, we have refitted the 1979 day 246 data again, but forcing the ice parameter to its extreme values at ±20 per cent of nominal. We find that increasing the ice parameter produces a decrease in N_H of 2×10^{20} cm^{-2} and an increase in the mass deposition rate of 600 $M_\odot$ yr^{-1}. Decreasing the ice parameter increases N_H by 1×10^{20} cm^{-2} and decreases the mass deposition rate by 114 $M_\odot$ yr^{-1}. The corresponding increases in chi-square are 1.0 and 0.3 respectively. We are therefore confident that the measurement of the large excess column density of $N_H\sim2.5\times10^{21}$ cm^{-2} is not significantly affected by errors in the ice correction. The significance of the cooling flow component is, however, somewhat less than the formal 95 per cent level quoted above.

5 DISCUSSION

Analysis of the *Einstein* HRI image of Abell 478 by Arnaud (1986) and Thomas *et al.* (1987), and the *EXOSAT* LE image by Edge & Stewart (1991), assuming the galactic column density of 1.3×10^{21} cm^{-2}, indicated the presence of a cooling flow of ~550 $M_\odot$ yr^{-1}. Using this value of column density, we find that the *Ginga* data are inconsistent with such a cooling flow. The *Ginga* data become marginally consistent with a flow of ~550 $M_\odot$ yr^{-1} if the absorption column is near the corrected value inferred from the 21-cm neutral hydrogen observations, $N_H=2\times10^{21}$ cm^{-2}. However, the two data sets become much more consistent if the mass deposition rate and the absorption column density are increased. The SSS data which originate from the inner ~450 kpc (3 arcmin) radius region of the cluster confirm that the absorption column lies in the range ~4–5×10^{21} cm^{-2}, with the mass deposition rate between 100 and 1470 $M_\odot$ yr^{-1}. All three data sets are in good agreement with $N_H\sim4.8\times10^{21}$ cm^{-2} and $\dot{M}\sim1000$ $M_\odot$ yr^{-1} (Fig. 2).

There are two obvious interpretations of the high column density measured from the X-ray observations. First, it may be due to an underestimate of galactic absorption, since the absorption column measured from the H I 21-cm observations is interpolated from a $2°\times2°$ grid of measurements and there is a reflection nebulosity close by which may contribute extra absorption on small spatial scales.

The other possibility is that the absorption is intrinsic to the cluster. In this case, the absorbing column must be corrected for the redshift of the cluster. Assuming, to first order, that the absorption has an exponential form, the intrinsic absorption is higher by a factor of $(1+z)^3$, giving 3.6×10^{21} cm^{-2}. If the gas which is cooling in the central regions does not efficiently form stars, then there may be a substantial column density of cold gas within the cooling radius. A simple estimate of the column density that could result from a cooling flow, on the assumption that the gas is spread uniformly throughout the volume in which it is deposited, is

$$N_H=\frac{M}{m_H}\frac{1}{\pi r_{cool}^2},$$

where M is the total mass deposited within r_{cool}, the cooling radius. A cooling flow with a mass deposition rate of 1000 $M_\odot$ yr^{-1}, persisting for $\sim4\times10^9$ yr throughout a region with radius 200 kpc, would give a column density of $N_H\sim4\times10^{21}$ cm^{-2}, which is similar to the extra column observed in Abell 478.

For a mass deposition rate of 1000 $M_\odot$ yr^{-1} cooling from the measured cluster temperature of 6.8 keV, the 2–10 keV luminosity is 5.4×10^{44} erg s^{-1}. This is only 23 per cent of the 2–10 keV luminosity inferred from the *Ginga* data, or 33 per cent of that inferred from the SSS. Thus 67 per cent of the luminosity seen by the SSS must come from the ambient cluster gas. (The relatively high redshift of this cluster means that a relatively small fraction of the SSS luminosity is contributed by the cooling flow. This, in part, accounts for the relatively poor sensitivity of the spectra to the cooling flow. The situation is exacerbated by the absorption of the low-energy flux where we expect to see the distinctive signature of the cooling flow.) If equal fractions of the observed flux come from in front of and behind the cooling flow with some contribution from outside the cooling region, then the intrinsic column density must be higher than that measured. In fact, a partial covering model is needed in which only part of the ambient cluster gas and part of the cooling flow emission is absorbed. It may be, however, that a higher mass deposition rate in the past is required to give the extra measured absorption. Forbes *et al.* (1990) have shown that cooling flows detected around quasars up to redshifts of $z\sim1$ have larger mass deposition rates than most nearby cooling flows.

We are unable to determine whether the excess absorption in Abell 478 is intrinsic to the cluster or associated with our Galaxy, although White *et al.* (1991) have shown that the presence of excess absorption is common among clusters. Future higher spectral and spatial resolution observations may be able to distinguish between the two possibilities, either through measurements of the redshift of the absorption edges or by showing a detailed spatial correspondence between absorption and the cooling flow region. If the absorption is found to be associated with the cooling flow then more complex, partial covering models will be needed to interpret both spectral and imaging data from clusters.

5.1 The maximum mass deposition rate and inhomogeneous gas in Abell 478

Cooling flows are inhomogeneous, otherwise a much more strongly peaked surface brightness profile would be observed* (Fabian *et al.* 1984; Nulsen 1986; Thomas *et al.* 1987). The gas must consist of an emulsion of blobs of different densities at each radius within the region where the surface brightness is peaked. The blobs are in pressure equilibrium with each other (at each radius) and the densest (and therefore at lowest temperature) cool out of the flow just within that radius. The mass deposition is distributed throughout the cooling region in a manner which reflects the distribution of temperatures of the blobs in the cooling gas.

* The measured absorption column density corresponds to a cut-off at energies below ~1 keV, so that less than 50 per cent of the HRI flux will be absorbed. This distributed absorption will not significantly affect the mass deposition profile, $\dot{M}\propto r$, which is derived from the surface brightness distribution at higher energies.

The cooling radius then corresponds to that radius where the *average* cooling time corresponds to the age of the cluster. There may still be dense gas blobs cooling beyond this region.

We can easily set an upper limit on the total amount of inhomogeneous cluster gas since the temperature distribution is likely to resemble that in the cooling gas (Thomas *et al.* 1987). The *Ginga* LAC sees the whole of the cluster emission so that the maximal cooling flow component which can be fitted to the spectrum will measure not only that gas cooling within $r_{\rm cool}$ but also any gas beyond $r_{\rm cool}$ which has a range of temperatures and densities. Just beyond the cooling radius, this gas may be cooling from close to the cluster temperature, but much further out it is likely that this gas is at too low a pressure to cool and represents the initial density fluctuations in the cluster, however they were formed.

On the assumption that the absorption column is 4.5×10^{21} cm^{-2} as measured from the SSS data, the *Ginga* data give a mass deposition rate of 907^{+390}_{-398} $M_\odot$ yr^{-1} (90 per cent confidence region for a single parameter). The 90 per cent confidence upper limit to the mass deposition rate is then ~1300 $M_\odot$ yr^{-1}. Comparison of this upper limit with the lower bound on the error bar from the HRI deprojection at 800 $M_\odot$ yr^{-1} (assuming again that $N_{\rm H}=4.5\times10^{21}$ cm^{-2}) means that the luminosity from the inhomogeneities beyond $r_{\rm cool}$ can correspond at most to the enthalpy released by 500 $M_\odot$ yr^{-1} of gas cooling from $T_{\rm cluster}=6.8$ keV, or $L_{\rm bol}=8.7\times10^{44}$ erg s^{-1}. This is about one sixth of the total cluster luminosity measured by *Ginga*.

If the hot and cool gas components are spatially distributed in the same manner, then the relative masses of gas with luminosities L_1, L_2, electron densities n_1, n_2 and temperatures T_1, T_2 are given approximately by

$$\frac{M_1}{M_2}=\frac{L_1}{n_1\Lambda(T_1)}\Big/\frac{L_2}{n_2\Lambda(T_2)},$$

where $\Lambda(T)$ is the cooling function at temperature T. If the two phases are in pressure equilibrium and the cooling function above $kT\sim1.7$ keV is parametrized as $\Lambda(T)\propto T^{0.4}$ as in Thomas (1987), then

$$\frac{M_1}{M_2}=\frac{L_1}{L_2}\frac{T_1^{0.6}}{T_2^{0.6}}.$$

If the average temperature in the distribution of denser phases is close to half the cluster temperature, then the upper limit on the fraction of cluster mass which is inhomogeneous is ~10 per cent. This limit will be even tighter if the cool gas is concentrated around the edge of the cooling region. Most of the intracluster gas must therefore be isothermal and homogeneous.

6 CONCLUSIONS

We have presented a new *Ginga* spectrum of the cluster Abell 478. A simple analysis indicates that the data are well fitted by an isothermal emission model with a temperature $kT=6.8$ keV and metal abundances of 0.37 times the solar values with a luminosity of 2.3×10^{45} erg s^{-1}. We set a limit on the 2–10 keV luminosity of 6.3×10^{43} erg s^{-1} of any absorbed power-law continuum component which has a spectral index typical of active galactic nuclei.

The *Ginga* data superficially do not require the presence of the cooling flow evident from the highly peaked X-ray images if a value for the galactic absorption of $N_{\rm H}\sim2\times10^{21}$ cm^{-2}, based on 21-cm observations of H I is adopted. We find, however, that the *Einstein* SSS data require a much higher column density, near 4.5×10^{21} cm^{-2}.

The mass deposition rates measured from the LAC, SSS and HRI are all consistent with $\dot{M}\sim1000$ $M_\odot$ yr^{-1}, provided that the absorbing column is $N_{\rm H}\sim4.8\times10^{21}$ cm^{-2}. We are unable to determine whether the excess absorption is due to our Galaxy or whether it is intrinsic to the cooling flow.

ACKNOWLEDGMENTS

ACF and ACE thank the Royal Society for financial support.

REFERENCES

Arnaud, K. A., 1986. *PhD thesis,* University of Cambridge, UK.
Arnaud, K. A., 1988. *Cooling Flows in Clusters and Galaxies,* p. 35, ed. Fabian, A. C., Kluwer, Dordrecht.
Arnaud, K. A., Szymkowiak, A. E. & White, N., 1989. HEAO Newsletter, **1,** No. 2. *Einstein* Data Center, SAO, Cambridge Mass.
Arnaud, K. A., Johnstone, R. M., Fabian, A. C., Crawford, C. S., Nulsen, P. E. J., Shafer, R. A. & Mushotzky, R. F., 1987. *Mon. Not. R. astr. Soc.,* **227,** 241.
Canizares, C. R., Markert, T. H. & Donahue, M. E., 1988. *Cooling Flows in Clusters and Galaxies,* p. 63, ed. Fabian, A. C., Kluwer, Dordrecht.
Centurion, M. & Vladido, G., 1989. *Astr. Astrophys.,* **218,** 243.
Edge, A. C. & Stewart, G. C., 1991. *Mon. Not. R. astr. Soc.,* **252,** 414.
Edge, A. C., Stewart, G. C. & Fabian, A. C., 1992. *Mon. Not. R. astr. Soc.,* submitted.
Fabian, A. C., Nulsen, P. E. J. & Canizares, C. R., 1984. *Nature,* **310,** 733.
Fabian, A. C., Nulsen, P. E. J. & Canizares, C. R., 1991. *Astr. Astrophys. Rev.,* **2,** 191.
Fabian, A. C., Hu, E. M., Cowie, L. L. & Grindlay, J., 1981. *Astrophys. J.,* **248,** 47.
Forbes, D. A., Crawford, C. S., Fabian, A. C. & Johnstone, R. M., 1990. *Mon. Not. R. astr. Soc.,* **244,** 680.
Giacconi, R. *et al.,* 1979. *Astrophys. J.,* **230,** 540.
Hayashida, K., Inoue, H., Koyama, K., Awaki, H., Takano, S., Tawara, Y., Williams, O. R., Denby, M., Stewart, G. C. & Ohashi, T., 1989. *Publs astr. soc. Japan,* **41,** 373.
Holt, S. S., White, N. E., Becker, R. H., Boldt, E. A., Mushotzky, R. F., Serlemitsos, P. J. & Smith, B. W., 1979. *Astrophys. J. Lett.,* **234,** L65.
Hughes, J. P., Yamashita, K., Okumura, Y., Tsunemi, H. & Matsuoka, M., 1988. *Astrophys. J.,* **327,** 615.
Mitchell, R. J. & Mushotzky, R. F., 1980. *Astrophys. J.,* **236,** 730.
Morrison, R. & McCammon, D., 1983. *Astrophys. J.,* **270,** 119.
Mushotzky, R. F. & Szymkowiak, A. E., 1988. *Cooling Flows in Clusters and Galaxies,* p. 53, ed. Fabian, A. C., Kluwer, Dordrecht.
Nulsen, P. E. J., 1986. *Mon. Not. R. astr. Soc.,* **221,** 377.
Pesce, J. E., Fabian, A. C., Edge, A. C. & Johnstone, R. M., 1990. *Mon. Not. R. astr. Soc.,* **244,** 58.
Raymond, J. C. & Smith, B. W., 1977. *Astrophys. J. Suppl.,* **35,** 419.
Sarazin, C. L., 1986. *Rev. Mod. Phys.,* **58,** 1.
Stewart, G. C., Fabian, A. C., Jones, C. & Forman, W., 1984. *Astrophys. J.,* **285,** 1.

Szymkowiak, A. E., 1985. *PhD thesis,* University of Maryland, USA (also published as *NASA Technical Memorandum 86169*).
Thomas, P. A., 1987. *PhD thesis,* University of Cambridge, UK.
Thomas, P. A., Fabian, A. C. & Nulsen, P. E. J., 1987. *Mon. Not. R. astr. Soc.,* **228,** 973.
Turner, T. J. & Pounds, K. A., 1989. *Mon. Not. R. astr. Soc.,* **240,** 833.
Turner, T. J., Weaver, K. A., Mushotzky, R. F., Holt, S. S. & Madejski, G. M., 1991. *Astrophys. J.,* **381,** 85.
Valentijn, E. A. & Bijleveld, W., 1983. *Astr. Astrophys.,* **125,** 223.
White, D. A., Fabian, A. C., Johnstone, R. M., Mushotzky, R. F. & Arnaud, K. A., 1991. *Mon. Not. R. astr. Soc.,* **252,** 72.
Zabludoff, A. I., Huchra, J. P. & Geller, M. J., 1990. *Astrophys. J. Suppl.,* **74,** 1.